NASA Technical Memorandum 78795

ANALYTICAL MODELS AND SYSTEM TOPOLOGIES FOR REMOTE MULTISPECTRAL DATA ACQUISITION AND CLASSIFICATION

Friedrich O. Huck, Stephen K. Park, Ernest E. Burcher, and W. Lane Kelly IV

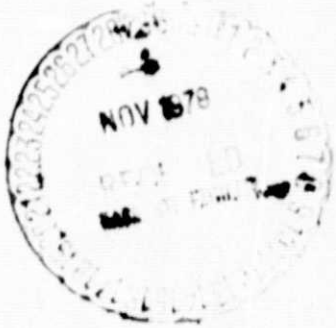

August 1978

National Aeronautics and Space Administration

Langley Research Center
Hampton, Virginia 23665

TABLE OF CONTENTS

TABLE OF CONTENTS - Concluded

ANALYTICAL MODELS AND SYSTEM TOPOLOGIES FOR REMOTE MULTISPECTRAL DATA ACQUISITION AND CLASSIFICATION

Friedrich O. Huck, Stephen K. Park, Ernest E. Burcher,
and W. Lane Kelly, IV
Langley Research Center

SUMMARY

This paper presents simple analytical models of the radiometric and statistical processes that are involved in multispectral data acquisition and classification. These models represent a preliminary but systematic step towards the use of computer simulations to gain a better understanding of the effect of major error sources on classification. This paper presents also some basic system topologies which combine remote sensing with data classification. Simulations of these topologies are intended to aid in the analysis of techniques for reducing classification errors and computations. However, before these models and topologies can be relied upon to yield useful results, they must be expanded to account more rigorously for target properties, atmospheric effects, and system component characteristics.

INTRODUCTION

There is a rapidly increasing demand for world-wide resource and environmental monitoring. This demand is currently met with several spacecraft multispectral imaging systems (such as Landsat) that transmit all acquired data (together with calibration data) to earth for processing in computer laboratories. Supporting studies tend to concentrate on specific aspects of remote sensing and data classification such as reflectance properties of objects, effects of the atmosphere, instrument technology, and data processing algorithms. Systematic analysis that account for all phases of the multispectral data acquisition and classification process and its error sources appear to be lacking, except for a recent study by Kondrat'yev et al. (ref. 1) in which remote sensing is analyzed from the viewpoint of information theory.

As the number of remote sensors and their spatial and spectral resolutions increase, the associated multispectral data transmission, storage, and processing requirements become excessively cumbersome and expensive to satisfy. Hence, it should become increasingly desirable to process multispectral data onboard the spacecraft itself. The onboard processing may initially be limited to editing; that is, for example, to the rejection of all data from clouds, or to the selection of all data containing information about vegetation.

This approach suggests a two-level decision process in which a simple level-1 decision process acts as a filter to reduce data loads for a more sophisticated level-2 decision process that classifies data, for example, as types of vegetation and soil. In fact, a two-level decision process may reduce the required number of computations in many applications as it has been demonstrated already for the classification of military targets (ref. 2).

As the reliance on remote sensing and data classification increases, it becomes also more important to better understand error sources in classification, and, if possible, to devise techniques for reducing their effect. Errors are introduced by variations of the spectral reflectance of various classes of objects, by variations in imaging conditions (such as atmospheric effects and lighting and viewing geometry) and imaging system response (such as calibration and noise), and by the models or training data used as reference patterns.

Limitations imposed on remote sensing by the atmosphere are particularly severe (ref. 3), and the compensation for atmospheric conditions has been strongly advocated (ref. 4). Initial investigations (refs. 5 to 9) indicate that compensation for atmospheric effects can indeed effectively reduce classification errors when signal patterns are acquired under atmospheric conditions that differ from those conditions that prevailed when training data were obtained.

In this paper we present simple analytical models of the complex radiometric and statistical processes that are involved in multispectral data acquisition and classification, and basic spacecraft system topologies which integrate these two functions. These models and topologies provide a preliminary but systematic approach for using computer simulations to gain a better understanding of the effect of major error sources on classification, and to aid in the analysis of techniques for reducing classification errors and computations.

SYMBOLS

$a_C(\lambda)$	selective absorption coefficient of carbon dioxide (CO_2), cm^{-1}
$a_H(\lambda)$	selective absorption coefficient of water vapor (H_2O), cm^{-1}
$a_O(\lambda)$	selective absorption coefficient of ozone (O_3), cm^{-1}
C_C	equivalent concentration of carbon dioxide (CO_2), cm
C_H	equivalent concentration of water vapor (H_2O), cm
C_O	equivalent concentration of ozone (O_3), cm
$C_N(\lambda, \lambda')$	covariance of spectral radiance

$C_\rho(\lambda, \lambda')$	covariance of spectral reflectance
c	sensitivity, $V\text{-}W^{-1}\text{-}cm^2\text{-}ster$
$c(\iota, \varepsilon)$	illumination scattering function, see equation (4)
D	dark current offset, V
H_0, H_1	hypothesis
I	number of picture elements per line
I( )	imaging conditions, see equations (22) and (31)
J	number of spectral channels, or dimensionality
L	number of classes of objects
M	number of broad categories of objects
MSD	mean-square distance, V^2, see equation (36)
N	number of classes of objects contained within a broad category
N_A	number density of aerosol integrated over height, km
N_R	number density of air molecules integrated over height, m^{-2}
$N(\lambda)$	spectral radiance, $W\text{-}cm^{-2}\text{-}\mu m^{-1}\text{-}sr^{-1}$
PDF	probability density function, see equation (38)
R	reference component, V, see equations (8), (17), and (18)
R'	reference component normalized for imaging condition, V, see equation (29)
S	error-free calibrated signal component, V, see equation (7)
S'	uncalibrated signal component, V, see equation (6)
S"	calibrated signal component, V, see equation (42)
$S(\lambda)$	solar spectral irradiance above earth atmosphere, $W\text{-}cm^{-2}\text{-}\mu m^{-1}$
$T(\lambda)$	normalized responsivity, see equation (5)
$V_N(\lambda)$	standard deviation of spectral radiance
$V_\rho(\lambda)$	standard deviation of spectral reflectance

Y	difference component between signal and reference, V, see equations (35) and (46)
$\alpha(\lambda)$	extinction optical thickness of atmosphere, see equation (2)
$\beta_A(\lambda)$	attenuation coefficient of aerosol, km^{-1}
$\gamma_{jj'}$	correlation element of reference signal, see equation (14)
$\delta(\ )$	delta or unit impulse function
ε	emittance angle, degree or radian
ε_c	sensitivity calibration error, V, see equation (44)
ε_d	dark current offset calibration error, V, see equation (45)
ε_r	radiometric calibration error, V, see equation (43)
θ	slant path angle, degree or radian
ι	incidence angle, degree or radian
Λ	spectral width of photosensor channel
λ	wavelength, μm
$\rho(\ )$	spectral reflectance, see equation (3)
σ_j	standard deviation element of reference pattern
$\sigma_{jj'}$	covariance element of reference pattern
$\sigma_R(\lambda)$	Rayleigh cross-section of air molecules, m^2
$\tau(\ )$	spectral transmittance of atmosphere, equation (1)

Subscripts:

i	picture element
j	spectral channel
ℓ	class of objects
m	broad category of objects
n	class of objects within a specified broad category

A bar ($\bar{}$) over a symbol indicates a pattern or vector.

The bracket < > around a parameter denotes expected mean value.

The bracket [ ] around a parameter denotes matrix.

The bars | | around a parameter denote determinants.

RADIOMETRIC MODEL

In this first section we present a simple radiometric model (see fig. 1) of solar irradiance, atmospheric transmittance, surface reflectance, and spacecraft imaging system response. The spectral region of interest is 0.3 to 3.0 μm. While this model cannot be relied upon to yield quantitatively accurate results, it can nevertheless be easily used to gain some insight into the dependence of classification errors on differences between (simulated) actual and predicted imaging conditions.

Solar Irradiance

The absolute solar spectral irradiance $S(\lambda)$ above the atmosphere is well known and changes slightly (less than 6 percent) with variations in the distance from sun to earth. We neglect these variations because their effect on a multispectral signal pattern is small. For examples, see references 10 and 11.

Atmospheric Transmittance

The atmospheric spectral transmittance $\tau(\lambda, \theta)$ changes in time and locality with variations in scattering and absorption by various particles and molecules. Atmospheric transmittance severely distorts the signal pattern, and hence limits the accuracy of its classification. We neglect the diffuse sky radiation of the scene and the atmospheric path radiance. Their effects are generally less significant for the lighting and viewing conditions that are desirable for multispectral imaging, but must eventually be accounted for to obtain more accurate quantitative results.

The slant-path transmittance of the atmosphere is (ref. 9)

$$\tau(\lambda, \theta) = e^{-\alpha(\lambda) \sec\theta}, \tag{1a}$$

where $\alpha(\lambda)$ is the extinction optical thickness along the vertical path from space to the earth surface, and $\sec\theta$ is the ratio of the length of the vertical path to the length of the slant path. The

slant angle $\theta = \iota$ for the incidence path, and $\theta = \varepsilon$ for the emittance path. For slant angles larger than 62°, corrections must be made for atmospheric refraction (ref. 7). To simplify notation, it is convenient to define $\tau(\lambda, \iota, \varepsilon)$ as

$$\tau(\lambda, \iota, \varepsilon) = \tau(\lambda, \iota)\tau(\lambda, \varepsilon) = e^{-\alpha(\lambda)(\sec\iota + \sec\varepsilon)} \tag{1b}$$

For the spectral region of interest, the atmospheric transmittance is primarily affected by Rayleigh scattering of air molecules (N_2 and O_2), Mie scattering of aerosols (water droplets and dust), and absorption by ozone (O_3), water vapor (H_2O), and carbon dioxide (CO_2) (refs. 7 and 9). We neglect the height profile of particle density and molecular concentration, and account for the total optical thickness as

$$\alpha(\lambda) = N_R\, \sigma_R(\lambda) + N_A\, \beta_A(\lambda) + D_O\, a_O(\lambda) + D_H\, a_H(\lambda) + D_C\, a_C(\lambda), \tag{2}$$

where N is column density, D is concentration, $\sigma_R(\lambda)$ is the Rayleigh cross-section of air molecules, $\beta_A(\lambda)$ is the attenuation coefficient of aerosol, and $a_O(\lambda)$, $a_H(\lambda)$, and $a_C(\lambda)$ are selective absorption coefficients, respectively, due to O_3, H_2O, and other uniformly mixed gases of which CO_2 has the dominant effect (ref. 10).

Surface Reflectance

The spectral reflectance $\rho(\lambda, \iota, \varepsilon)$ of a surface is generally a complex function of lighting and viewing geometry as well as wavelength. We neglect this complex dependence, and assume that the wavelength dependence of the spectral reflectance is independent of the incidence (ι) and emittance (ε) angle and that scattering is Lambertian. Hence,

$$\rho(\lambda, \iota, \varepsilon) = \rho(\lambda) \cos\iota \cos\varepsilon, \tag{3}$$

where $\rho(\lambda)$ is commonly referred to as spectral signature. Again, as for atmospheric effects, the surface reflectance must also be more realistically modeled to obtain useful quantitative results.

The classification of surface targets from multispectral image data relies on the observation that all physical and biological substances exhibit a uniquely characteristic spectral signature. Differences between spectral signatures may be easy to distinguish for diverse substances such as water, ice, dry sand, soil, and green vegetation. However, these differences tend to be very subtle and in practice often difficult to distinguish for related substances such as different types of crops. Moreover, the spectral signature of vegetation, for example, varies with such factors as moisture, season, soil, and growth density. Furthermore, various backgrounds can change the effective target radiance by a significant amount. For example, see references 10 and 14 to 21.

Spectral Radiance

Combining the solar irradiance, atmospheric transmittances, and surface reflectance, we formulate the radiance $N(\lambda, \iota, \varepsilon)$ sensed by a multispectral imaging system as

$$N(\lambda, \iota, \varepsilon) = S(\lambda)\tau(\lambda, \iota, \varepsilon)\rho(\lambda)\, c(\iota, \varepsilon), \tag{4}$$

where

$$c(\iota, \varepsilon) = \frac{1}{\pi} \cos\iota \cos\varepsilon.$$

Imaging System Response

We assume that the response $T_j(\lambda)$ of the j'th spectral channel of a J-channel multispectral imaging system is represented by the function

$$T_j(\lambda) = \begin{cases} \dfrac{1}{\Lambda_j}\left[1 - 3\left|\dfrac{\lambda - \lambda_j}{\Lambda_j}\right|^2 + 2\left|\dfrac{\lambda - \lambda_j}{\Lambda_j}\right|^3\right], & \left|\dfrac{\lambda - \lambda_j}{\Lambda_j}\right| \le 1 \\ 0, & \text{otherwise} \end{cases} \tag{5}$$

shown in figure 2. The center wavelength of $T_j(\lambda)$ is λ_j and the effective width is Λ_j. This function has been normalized so that

$$\int_0^\infty T_j(\lambda)\, d\lambda = 1.$$

Photosensor Signal

The imaging system generates a photosensor signal for the spectral radiance $N(\lambda,\iota,\varepsilon)$ that we represent as the J-dimensional vector (i.e., column matrix) $\bar{S}'$ with components

$$S_j' = c_j \int_0^\infty N(\lambda, \iota, \varepsilon) T_j(\lambda)\, d\lambda + D_j, \tag{6}$$

where c_j and D_j represent photosensor sensitivity and dark current offset, respectively. If sensitivity and offset variations are accounted for without error, then the components of the (calibrated) signal pattern $\bar{S}$ become

$$S_j = \frac{S_j' - D_j}{c_j} = \int_0^\infty N(\lambda, \iota, \varepsilon) T_j(\lambda)\, d\lambda \tag{7}$$

STATISTICAL MODELS

In this second section we present two statistical models (see figure 3) for reference patterns and covariance matrices: a common model in which imaging conditions are not accounted for, and a model in which they are accounted for to reduce classification errors.

Definitions

We regard for our two statistical models either the spectral radiance $N(\lambda, \iota, \varepsilon)$ or the spectral signature $\rho(\lambda)$ as a random process which for each λ has a Gaussian probability density distribution. It follows that the photosensor signal in each spectral channel has also a Gaussian probability density distribution since equations (6) and (7) relate it to these functions by a linear process.

We can define, therefore, the reference pattern for a class of objects (e.g., vegetation or wheat) as the J-dimensional vector $\bar{R}$ with components that are the expected (mean) signal value in each spectral channel as given by

$$R_j = E\{S_j\} = \langle S_j \rangle. \tag{8}$$

These components are the features of $\bar{R}$ that (hopefully) distinguish between signal patterns of various classes of objects. The associated covariance is given by the symmetric J-dimensional matrix $[\sigma_{jj'}]$ with elements

$$\sigma_{jj'} = E\{(S_j - \langle S_j \rangle)(S_{j'} - \langle S_{j'} \rangle)\} \tag{9}$$

The covariance matrix can also be written as the product

$$[\sigma_{jj'}] = [\sigma_j][\gamma_{jj'}][\sigma_{j'}]. \tag{10}$$

In this equation $[\sigma_j]$ is the diagonal matrix of the standard deviation

$$[\sigma_j] = \begin{bmatrix} \sigma_1 & 0 & \cdots & 0 \\ 0 & \sigma_2 & & 0 \\ \cdot & & & \cdot \\ \cdot & & & \cdot \\ \cdot & & & \cdot \\ 0 & 0 & \cdots & \sigma_J \end{bmatrix} \tag{11}$$

with elements

$$\sigma_j = \sqrt{\sigma_{jj}} \tag{12}$$

And $[\gamma_{jj'}]$ is the symmetric correlation matrix

$$[\gamma_{jj'}] = \begin{bmatrix} 1 & \gamma_{12} & \cdots & \gamma_{1J} \\ \gamma_{21} & 1 & & \gamma_{2J} \\ \cdot & & & \cdot \\ \cdot & & & \cdot \\ \cdot & & & \cdot \\ \gamma_{J1} & \gamma_{J2} & \cdots & 1 \end{bmatrix} \tag{13}$$

with elements

$$\gamma_{jj'} = \frac{\sigma_{jj'}}{\sigma_j \sigma_{j'}}. \tag{14}$$

Values of the non-diagonal correlation elements $\gamma_{jj'}$, $j \neq j'$, vary from 0 to 1, and may in practice sometimes be negative (ref. 22).

Model 1

General.- We define the expected (mean) value of the spectral radiance $N(\lambda, \iota, \varepsilon)$ for a normal incidence and emittance angle (i.e., $\iota = \varepsilon = 0$) as

$$E\{N(\lambda)\} = \langle N(\lambda) \rangle, \tag{15}$$

and the (auto-) covariance as

$$E\{[N(\lambda) - \langle N(\lambda) \rangle][N(\lambda') - \langle N(\lambda') \rangle]\} = C_N(\lambda, \lambda'). \tag{16}$$

The components of the reference pattern $\bar{R}$ become then

$$R_j = E\{\int_0^\infty N(\lambda)T_j(\lambda)\,d\lambda\} = \int_0^\infty \langle N(\lambda)\rangle T_j(\lambda)\,d\lambda, \tag{17}$$

and the elements of the covariance matrix $[\sigma_{jj'}]$ become

$$\sigma_{jj'} = E\{\int_0^\infty [N(\lambda) - \langle N(\lambda)\rangle]T_j(\lambda)\,d\lambda \int_0^\infty [N(\lambda') - \langle N(\lambda')\rangle]T_{j'}(\lambda')d\lambda'\}$$

$$= E\{\int_0^\infty \int_0^\infty [N(\lambda) - \langle N(\lambda)\rangle][N(\lambda') - \langle N(\lambda')\rangle]T_j(\lambda)T_{j'}(\lambda)d\lambda d\lambda'\}$$

$$= \int_0^\infty \int_0^\infty C_N(\lambda, \lambda')\, T_j(\lambda)\, T_{j'}(\lambda')\, d\lambda\, d\lambda'. \tag{18}$$

Special case.- If $N(\lambda)$, $N(\lambda')$ are uncorrelated and $V_N(\lambda)$ is the standard deviation of $N(\lambda)$, so that

$$C_N(\lambda,\lambda') = V_N^2(\lambda)\,\delta(\lambda - \lambda'), \tag{19}$$

then the covariance elements become

$$\sigma_{jj'} = \int_0^\infty V_N^2(\lambda)\, T_j(\lambda)\, T_{j'}(\lambda)\, d\lambda, \tag{20}$$

If, furthermore, the responses $T_j(\lambda)$, $T_{j'}(\lambda')$ do not overlap, then

$$\sigma_{jj'} = \begin{cases} \int_0^\infty V_N^2(\lambda)\, T_j^2(\lambda) d\lambda, & j = j' \\ 0, & j \neq j' \end{cases} \tag{21}$$

and the correlation matrix $[\gamma_{jj'}]$ reduces to an identity matrix.

Model 2

General.- We assume now that the imaging conditions which we denote as

$$I(\lambda, \iota, \varepsilon) = \tau(\lambda, \iota, \varepsilon)\, c(\iota, \varepsilon) \tag{22}$$

can be accounted for, and hence that the uncertainties associated with the spectral radiance $N(\lambda, \iota, \varepsilon)$ are caused only by the random process which generates the spectral signature $\rho(\lambda)$. The spectral radiance has then the expected (mean) value

$$E\{N(\lambda, \iota, \varepsilon)\} = \langle N(\lambda, \iota, \varepsilon)\rangle = S(\lambda)\, I(\lambda, \iota, \varepsilon)\, \langle \rho(\lambda)\rangle, \tag{23}$$

and (auto-) covariance

$$E\{[N(\lambda, \iota, \varepsilon) - \langle N(\lambda, \iota, \varepsilon)\rangle][N(\lambda', \iota, \varepsilon) - \langle N(\lambda', \iota, \varepsilon)\rangle]\}$$

$$= S(\lambda)S(\lambda')I(\lambda,\iota,\varepsilon)I(\lambda',\iota,\varepsilon)C_\rho(\lambda,\lambda'). \tag{24}$$

Substituting equations (23) and (24) into equations (17) and (18) yields the reference pattern components

$$R_j = \int_0^\infty S(\lambda)\, I(\lambda, \iota, \varepsilon) \langle\rho(\lambda)\rangle T_j(\lambda)\, d\lambda, \tag{25}$$

and covariance elements

$$\sigma_{jj'} = \int_0^\infty \int_0^\infty S(\lambda)S(\lambda')I(\lambda,\iota,\varepsilon)I(\lambda',\iota,\varepsilon)C_\rho(\lambda,\lambda')T_j(\lambda)T_{j'}(\lambda')d\lambda d\lambda'. \tag{26}$$

Approximation.- To reduce the number of computations required for atmospheric compensation, it might generally be desirable to approximate equations (25) and (26), respectively, as

$$R_j = I_j(\iota, \varepsilon)\, R_j' \tag{27}$$

and

$$\sigma_{jj'} = I_j(\iota, \varepsilon)\, I_{j'}(\iota,\varepsilon)\sigma'_{jj'}, \tag{28}$$

where

$$R_j' = \int_0^\infty S(\lambda) \langle\rho(\lambda)\rangle\, T_j(\lambda)\, d\lambda, \tag{29}$$

$$\sigma'_{jj'} = \int_0^\infty \int_0^\infty S(\lambda)S(\lambda')C_\rho(\lambda,\lambda')T_j(\lambda)T_{j'}(\lambda')d\lambda d\lambda', \tag{30}$$

and

$$I_j(\iota, \varepsilon) = c(\iota, \varepsilon) \int_0^\infty \tau(\lambda, \iota, \varepsilon)\, T_j(\lambda)\, d\lambda. \tag{31}$$

That is, $\bar{R}'$ and $[\sigma'_{jj'}]$ are the reference pattern and covariance matrix, respectively, that represent the multispectral features of a class of objects, and $I_j(\iota, \varepsilon)$ is the factor by which these functions are corrected to account for imaging conditions.

Special case.- If $\rho(\lambda)$, $\rho(\lambda')$ are uncorrelated and $V_\rho(\lambda)$ is the standard deviation of $\rho(\lambda)$, so that

$$C_\rho(\lambda, \lambda') = V_\rho^2(\lambda)\, \delta(\lambda - \lambda'), \tag{32}$$

then the covariance elements become

$$\sigma'_{jj'} = \int_0^\infty S^2(\lambda)\, V_\rho^2(\lambda)\, T_j(\lambda) T_{j'}(\lambda)\, d\lambda. \tag{33}$$

If, furthermore, the responses $T_j(\lambda)$, $T_{j'}(\lambda')$ do not overlap, then

$$\sigma'_{jj'} = \begin{cases} \int_0^\infty S^2(\lambda)\, V_\rho^2(\lambda)\, T_j^2(\lambda) d\lambda, & j = j' \\ 0, & j \neq j'. \end{cases} \tag{34}$$

CLASSIFICATION MODELS

Classification is essentially a process that assigns a large number of signal patterns $\bar{S}$ to a small number of reference patterns $\bar{R}$. In this third section we present two types of classification decisions: one decision uses the minimum mean-square distance between the signal and reference pattern, and the other decision uses the maximum-likelihood ratio. The latter is the optimum target detection process in many applications, and is most commonly used in the classification of multispectral data.

Mean-Square Distance

We let $\bar{S}_i$ be the signal pattern of pixel i, $\bar{R}_\ell$ be the reference pattern of a class of objects ℓ, and $\bar{Y}_{\ell i}$ be the J-dimensional difference vector between these two patterns with components

$$Y_{\ell ij} = S_{ij} - R_{\ell j} . \tag{35}$$

The mean-square distance (MSD) between a signal and reference pattern is then given by

$$MSD_{\ell i} = \bar{Y}_{\ell i}^T \bar{Y}_{\ell i} = \sum_{j=1}^{J} Y_{\ell ij}^2 . \tag{36}$$

The classification decision is to select the reference pattern for which the mean-square distance is smallest, that is, for which

$$MSD_{\ell' i} < MSD_{\ell i} , \tag{37}$$

where $\ell = 1, 2, \ldots, L$ but $\ell \neq \ell'$, and L is the total number of classes.

Maximum-Likelihood Ratio

General.- The J-dimensional Gaussian probability density function (PDF) for computing the likelihood that the signal pattern $\bar{S}_i$ belongs to the class of objects ℓ is given by

$$PDF_{\ell i} = (2\pi)^{-J/2} |\sigma_{\ell jj'}|^{-1/2} \exp\left\{ -\frac{1}{2} (\bar{Y}_{\ell i}^T [\sigma_{\ell jj'}]^{-1} \bar{Y}_{\ell i}) \right\}, \tag{38}$$

where $|\sigma_{\ell jj'}|$ is the determinant of the covariance matrix. The $PDF_{\ell i}$ is maximum when the signal pattern $\bar{S}_i$ and reference pattern $\bar{R}_\ell$ coincide (i.e., when $Y_{\ell ij} = 0$ for all j), and smootnly decreases with increasing separation between these two patterns at a rate that is controlled by the covariance.

The logarithm of the $PDF_{\ell i}$ given by

$$\ell n\ PDF_{\ell i} = -\frac{1}{2} (J\ \ell n\ 2\pi + \ell n |\sigma_{\ell jj'}| + \bar{Y}_{\ell i}^T\ [\sigma_{\ell jj'}]^{-1}\ \bar{Y}_{\ell i}) \tag{39}$$

is commonly used to avoid the computation of an exponential. The classification decision is then to select the reference pattern for which

$$|\ell n\ PDF_{\ell' i}| < |\ell n\ PDF_{\ell i}| \tag{40}$$

where $\ell = 1, 2, \ldots, L$ but $\ell \neq \ell'$. The term $J\ \ell n\ 2\pi$ can be neglected if J is constant for all decisions, as is usually the case.

Special case.- If the components of the reference pattern $\bar{R}_\ell$ are uncorreiated, and hence the covariance matrix $[\sigma_{\ell jj'}]$ reduces to a diagonal matrix with eiements given by equations (21) and (34) for the two statistical models, then the computation of equation (39) reduces to

$$\ell n\ PDF_{\ell i} = -\frac{1}{2} \left(\sum_{j=1}^{J} \ell n\ \sigma_{\ell jj} + \sum_{j=1}^{J} \frac{Y_{\ell ij}^2}{\sigma_{\ell jj}} \right). \tag{41}$$

ERROR MODELS

In this fourth section we show how the radiometric and statistical models can be used to simulate the effect of errors in radiometric calibration and atmospheric compensation on classification. Variations of the spectral signatures of a class of targets are already accounted for by the covariance matrix $[\sigma_{\ell jj'}]$.

Types of Errors

Consider the following hypothesis and its alternative:

$$H_0: \ \bar{S}_i \ \xi \ \bar{R}_\ell$$

$$H_1: \ \bar{S}_i \ \not\xi \ \bar{R}_\ell$$

There are two types of associated errors: the type I error which is to reject H_0 when in fact H_0 is true (i.e., when $\rho_i(\lambda) \ \xi \ \rho_\ell(\lambda)$), and the type II error which is to accept H_0 when in fact H_1 is true (i.e., when $\rho_i(\lambda) \not\xi \rho_\ell(\lambda)$).

Radiometric Calibration

We let c_{ij} and D_{ij} be the actual values of photosensor sensitivity and dark current offset, respectively, and $\langle c_j \rangle$ and $\langle D_j \rangle$ be their expected values (i.e., the calibration data). The components of the calibrated signal pattern $\bar{S}_i$ are then given by

$$S''_{ij} = \frac{S'_{ij} - \langle D_j \rangle}{\langle c_j \rangle} = \frac{c_{ij}}{\langle c_j \rangle} S_{ij} + \frac{D_{ij} - \langle D_j \rangle}{\langle c_j \rangle}, \tag{42}$$

where S'_{ij} are the components of the photosensor signal given by equation (6), and S_{ij} are the components of the error-free calibrated signal given by equation (7). The components of the radiometric calibration error pattern $\bar{\varepsilon}_{ri}$ are then given by

$$\varepsilon_{rij} = S''_{ij} - S_{ij} = \varepsilon_{cij} S_{ij} + \varepsilon_{dij}, \tag{43}$$

where

$$\varepsilon_{cij} = \frac{c_{ij} - \langle c_j \rangle}{\langle c_j \rangle} \tag{44}$$

and

$$\varepsilon_{dij} = \frac{D_{ij} - \langle D_j \rangle}{\langle c_j \rangle} \tag{45}$$

Hence, we can account for the effect of errors in radiometric calibration on data classification by reformulating the components of the difference vector $\bar{Y}_{\ell i}$ given by equation (35) as

$$Y_{\ell ij} = S_{ij} - R_{\ell j} + \varepsilon_{rij}. \tag{46}$$

Atmospheric Transmittance

If we do not attempt to compensate for atmospheric transmittance, then the components of the vector distance between signal and reference pattern become

$$S_{ij} - R_{\ell j} = \int_0^\infty [N_i(\lambda, \iota, \varepsilon) - \langle N_\ell(\lambda, \iota, \varepsilon)\rangle] \, T_j(\lambda) \, d\lambda \qquad (47)$$

If, however, we could compensate for imaging conditions without any error, then

$$S_{ij} - R_{\ell j} = \int_0^\infty S(\lambda) \;\; I_i(\lambda, \iota, \varepsilon)[\rho_i(\lambda) - \langle \rho_\ell(\lambda)\rangle] \, T_j(\lambda) \, d\lambda \qquad (48)$$

In practice, we can expect to introduce some error into the atmospheric compensation process by errors involved in estimating the concentration of atmospheric constituents and in simplifying computations by an approximation. In this case,

$$S_{ij} - R_{\ell j} = S_{ij} - \langle I_j(\iota, \varepsilon)\rangle \, R'_{\ell j}$$

$$= \int_0^\infty S(\lambda) I_i(\lambda, \iota, \varepsilon) \rho_i(\lambda) T_j(\lambda) d\lambda - \langle I_j(\iota, \varepsilon)\rangle \int_0^\infty S(\lambda) \, \langle \rho_\ell(\lambda)\rangle T_j(\lambda) d\lambda, \quad (49)$$

where the estimated imaging conditions are given by

$$\langle I_j(\iota, \varepsilon)\rangle = \langle c(\iota, \varepsilon)\rangle \int_0^\infty \langle \tau(\lambda, \iota, \varepsilon)\rangle \, T_j(\lambda) d\lambda.$$

SYSTEM TOPOLOGIES

In this fifth section we present three system topologies (see figure 4) for classification: one topology represents the usual single-level decision process, and the other two topologies represent two-level decision processes for reducing the number of computations required for classification.

Decision Levels

Single-level.- The single-level decision process shown in figure 4(a) classifies each signal pattern $\bar{S}_i$ as one of L reference patterns $\bar{R}_\ell$. The selected pattern is denoted $\bar{R}_{\ell' i}$. This process generates a spatial distribution of reference patterns that are generally highly redundant. The clustering process removes this redundancy by establishing regional boundaries for different reference patterns.

Two-level.- It may be advantageous in some applications to edit the incoming signal patterns; that is, to reject, for example, all data from clouds, or to accept all data from vegetation. In the two-level decision process shown in figure 4(b), a filter reduces data processing loads for a level-2 classifier by applying a simple decision rule to eliminate obvious cases from further consideration. Since the level-2 classifier needs to process only admissible classes, every time a signal pattern fails to be admissible, the level-2 data processing load is decreased (ref. 2).

A further sophistication is introduced by the system topology shown in figure 4(c). We assume that L reference patterns can be grouped into M broad categories (e.g., clouds, water, soil, and vegetation) with each category containing up to N reference patterns (e.g., types of soil and vegetation) so that $MN \geq L$. Reference patterns that represent broad categories are denoted $\bar{R}_m$, and reference patterns that belong to a selected category are denoted $\bar{R}_{m'n}$.

The supervisory (or level-1) classifier correlates all signal patterns with the reference patterns $\bar{R}_m$, and informs the reference pattern library of each selection R'_m. The library, in turn, sends the corresponding reference patterns $\bar{R}_{m'n}$ to the level-2 classifier for further correlation with the signal pattern. It might in some cases be efficient to separate the signal pattern $\bar{S}_i$ into two patterns, $\bar{S}_{1i}$ and $\bar{S}_{2i}$, with different spectral channels.

Computational Requirements

Table I summarizes the number of computations required to classify a signal pattern with the single and two-level decision process of figures 4(a) and (c), respectively, using either the mean-square distance (MSD) or maximum-likelihood ratio (MLR) decision process. For comparison, let us assume that $L = MN$ and $J_1 = J_2 = J$. The number of computations with the

single-level topology is then proportional to the product MN, and with the two-level topology is proportional to the sum $M + N$. Clearly, $\frac{MN}{M+N} > 1$ for $M > 2$, $N > 2$. For example, if $M = 4$ and $N = 10$, the single-level topology requires about three times as many computations as the two-level topology.

The two-level topology with a supervisory classifier provides still further opportunities for reducing the number of computations if only a limited number of broad categories are of interest so that the level-2 processing load is decreased each time a broad category is rejected, or if the classification of broad categories requires fewer spectral channels (so that $J_1 > J_2$) and/or a simpler decision process. Potential reductions in computational requirements must, of course, be carefully traded against increases in classification errors.

SYSTEM PERFORMANCE AND DESIGN MODELS

In this sixth and final section, we present an analytical model for the computer simulation of multispectral data acquisition and classification based on the foregoing models and topologies. We describe also some general spacecraft system design approaches and alternatives that are suggested by these models and topologies.

Analytical Model

Figure 5 shows an analytical model for simulating various system configurations for multispectral data acquisition and classification. The model provides the following options:

(1) Single-level classification, using either the minimum mean-square distance or maximum-likelihood decision process.

(2) Two-level classification, using the minimum mean-square distance decision process for supervisory classification and the maximum-likelihood decision process for level 2 classification.

(3) Either one of the above topologies with or without compensation for imaging conditions.

To simulate clustering, we use the simple process of run-length encoding. The run-length encoder compares each selected reference pattern $R_{m'i}$ (or $R_{m'n'i}$) with the preceding pattern $R_{m'i-1}$ (or $R_{m'n'i-1}$). It passes each new pattern $R_{m'i} \neq R_{m'i-1}$, and counts each repetitive pattern $R_{m'i} = R_{m'i-1}$. Two-dimensional clustering algorithms that have been developed (refs. 24 to 28) are beyond the scope of our model.

Design Considerations

Figure 6 shows a typical spacecraft imaging geometry, and figure 7 shows a compatible signal processing flow diagram. The system uses the two-level decision topology with a single supervisory classifier and several level 2 classifiers. This topology offers not only some opportunities for reducing computational requirements and rates, but also a wide range of alternatives for the application of various technologies. Several level 2 classifiers versus only a single supervisory classifier might be desirable since the level 2 classifiers must generally distinguish between more subtle differences in signal patterns.

In addition to classification, the diagram accounts for a buffer memory, radiometric calibration, spatial registration of multispectral data, compensation for imaging conditions, and clustering of classified data. Data processing might be performed either with analog samples, digital data, or a hybrid system in which, for example, the supervisory classifier may use integrated optics technology and the level 2 classifiers may use digital or charge-coupled devices technology. Compensation for imaging conditions on the reference patterns rather than on the signal patterns promises fewer computations simply because there are fewer reference patterns than signal patterns.

The system topology is compatible with various imaging techniques. We assume that the imaging system provides an image sampling lattice of I pixels normal to the spacecraft flight path, and J spectral channels along the flight path (see figure 6).

In an optical-mechanical scanner, J photosensors, each covered by a spectral filter, would be located along the flight path direction, and a servo-controlled mirror would scan an image of the scene past these photosensors in a direction that is normal to the flight path. The analog signals that are generated along the line-scan direction would be electronically sampled.

In a pushbroom scanner, J linear photosensor arrays, each covered by a spectral filter and connected to a transport array, would be oriented normal to the flight path direction. The signals from the I photosensors of each array would be periodically transferred in parallel to an associated transport array, and nearly continuously readout in series from each transport array.

The sequence of the spectral channels should be ordered according to their use in the classification process. The first J_1 channels are intended for the supervisory classifier, and the $J_2(\leq J)$ channels for the level 2 classifiers.

Other image-sampling lattices could also be advantageous. For example, a spatial separation between the first J_1 channels and the remaining $J-J_1$ channels could provide an increased delay between the two levels of classifications. Or even two separate photodetection mechanisms could be envisioned: one mechanism for the supervisory classifier that would be,

for example, optimized for speed (perhaps at the cost of spectral and/or spatial resolution), and the other for level 2 classifiers that would be optimized for spectral resolution. This arrangement could conceivably lead to a change in the basic topology to permit the supervisory classifier to select different spectral channels and resolutions for the level 2 classifiers.

A buffer memory may be required to match a high data acquisition rate to a slower data processing rate and/or to change a discontinuous data acquisition rate to a constant rate for continuous data processing. Typically, the buffer might accept (or read) data during the active cycle of each line scan and transmit (or write) the same data at a slightly reduced rate during the complete (active plus passive) line-scan period. In general, it appears to be desirable to match a continuous data processing rate to the average data acquisition rate so that the required storage capacity does not become excessively large.

Calibration requirements of the multispectral signal will depend on the performance characteristics of the photosensors. But two typical processes can be anticipated: one is subtraction of dark current offsets, and the other is multiplication by calibration constants.

The image-sampling lattice requires that the data from all but the last spectral channel must be delayed for proper spatial registration. Data from the first J_1 spectral channels must be synchronized for the supervisory classifier, and must also be synchronized together with data from the remaining channels for the level 2 classifiers. (It might be desirable to include these delays into the buffer memory.)

These delays could also provide corrections for geometric distortions called path skewing that are introduced if the spatial coverage normal to the flight path is obtained time sequentially (e.g., by an optical-mechanical scanner) rather than simultaneously (e.g., by a pushbroom scanner).

Conceptually, the simplest approach is to let the supervisory classifier wait until all data from the J_1 spectral channels have been synchronized before starting its classification task, and similarly to let the selected level 2 classifier wait until the data from all J_2 channels have been synchronized. However, a classifier might also start its task as soon as data from two or more spectral channels have been synchronized, and use data from the following channels as they become available. The latter approach might offer some saving in time and in delay requirements.

The supervisory and each level 2 classifier is anticipated to perform parallel correlations of the signal and reference patterns, and to identify the reference patterns that correlate most closely to the signal patterns. The result of the supervisory classification, which occurs first, is used to select the reference patterns for the level 2 classification, and the result of this classification is passed to a sequencing buffer.

The buffer sequences the selected reference codes into proper order. Correct sequencing could be obtained either by sending the selected patterns in proper order to the buffer or by using synchronizing signals that allow the buffer to arrange these patterns in proper order. The first approach appears conceptually easier. It could be implemented by multiplexing the incoming data to K level 2 classifiers together with the selected set of level 2 reference patterns. This scheme would assure that each level 2 classifier would continuously process data at a rate that is a factor of K slower than the basic data rate, and that the proper spatial sequence of the selected level 2 reference patterns could be easily maintained. To assure synchronization at the beginning of each scan line, it might be advantageous to let the ratio I/K be an integer so that the first pixel in each line is always processed by the first level 2 classifier.

It is the function of the clustering process to remove the data redundancy that results from classifying a large number of multispectral signal patterns into a few reference patterns. The simplest type of clustering is presented by the run-length encoder which reduces redundancy only along the line-scan direction (i.e., normal to the flight path). Its output consists of a succession of different pattern codes, eacn followed by the number of pixels for which the code was selected. A substantially more significant redundancy reduction could be accomplished with two-dimensional clustering algorithms, such as described and formulated in references 20 to 24.

Compensation for atmospheric conditions might increase the accuracy of multispectral data classification more than any other advances in processing techniques for remote sensors. Two efforts have been advocated to achieve this (ref. 4): development of improved atmospheric models for computing atmospheric attenuation, and development of instruments for measuring atmospheric optical quantities simultaneously with remote sensing observations.

Probably the simplest approach for estimating atmospheric effects would be to measure atmospheric conditions directly from periodically monitored targets concurrent with remote sensing observations (see, for example, ref. 5). Our approach to compensate for atmospheric transmittance suggests optical instruments that measure atmospheric attenuation in the same spectral bands as used by the spacecraft imaging system. The spacecraft could trigger any ground-based instrument within its viewing range to make an atmospheric measurement and transmit the result to the spacecraft. An obvious disadvantage of this approach would be the requirement for a large number of optical instruments with a signal reception and transmission capability. This disadvantage would be further compounded by platform requirements for oceans.

It would, therefore, probably be more desirable to augment the spacecraft imaging system itself with an electro-optical device for measuring optical properties of the atmosphere even if the measurement and signal processing technique is substantially more complex. The most important effects of atmospheric transmittance on the spectral radiance sensed by an earth-viewing imaging system could be distinguished from surface

reflectance properties by their relatively narrow absorption features (mostly due to H_2O and CO_2) at well-defined wavelengths. Atmospheric transmittance due to scattering varies relatively slowly with wavelength and can, therefore, not be so easily distinguished, but its distorting effect on the multispectral signal features is fortunately for the same reason less significant. Furthermore, it is the concentration of water vapor, and hence absorption, that varies most rapidly with time and locality, whereas scattering due to particles and molecules (and, incidentally, absorption due to CO_2) are more constant. All this suggests that major deformations due to the atmosphere could be estimated with an atmospheric model and measurements of the depth of a single absorption band for each constituent that is to be accounted for. Atmospheric modeling has the added advantage that it can account for atmospheric conditions that cannot be readily measured from the spacecraft but that can be obtained from other observations.

CONCLUDING REMARKS

Computer simulations of the analytical models and system topologies presented in this paper are intended to provide a better understanding of the effect of major error sources on multispectral data classification, and to aid in the selection of spectral bands and the evaluation of various system topologies and special remote sensing techniques such as atmospheric compensation. However, the analytical models must be expanded to account more rigorously for atmospheric effects, target properties, and system component characteristics before their simulations can be relied upon to yield definitive results.

Atmospheric effects must include sky radiation and path radiance as well as transmittance; target properties must include statistics about the reflectances of various classes of objects and the dependence of these statistics on lighting and viewing geometry; and system characteristics must include realistic assessments of photosensor sensitivity and noise and of the transfer functions of analog and digital electronics and of such new technologies as integrated optics if and when they become available. This requires not only the consolidation of existing data about atmospheric effects and object reflectances, but also more extensive measurements and modeling of these properties. Such a systematic and comprehensive approach can be expected to lead to more efficient system designs for earth resource and environmental monitoring.

REFERENCES

1. Kondrat'yev, K. Ya.; Grigor'yev, Al. A.; and Pokrovskiy, O. M.: Information Content of the Data Obtained by Remote Sensing of the Parameters of the Environment and the Earth's Resources from Space. Izdatel'stvo Leningradskogo Universiteta, 17 February 1975, NASA TT F-16435.

2. Proceedings of the 1970 IEEE Symposium on Adaptive Processes (9th) Decision and Control. The University of Texas at Austin, December 7-9, 1970.

3. Fraser, R. S.; and Curran, R. J.: Effects of the Atmosphere on Remote Sensing, in Remote Sensing of Environment, eds. J. Lintz and D. S. Simonsett, Addison-Wesley Publishing Company, 1976, pp. 65 to 67.

4. Advanced Scanners and Imaging Systems for Earth Observations. NASA SP-335, 1973.

5. Rogers, R. H.; Peacock, K.; and Shah, N. J.: A Technique for Correcting ERTS Data for Solar and Atmospheric Effects. Third Earth Resources Tech. Satellite Symp. I(B), 1973, pp. 1787-1804.

6. Potter, J. F.: Haze and Sun Angle Effects on Automatic Classification of Satellite Data - Simulation and Correction. Proceedings of the Photo-Optical Instrumentation Engineers, 51, 1974, pp. 73-83.

7. Turner, R. E.; Malila, W. A.; Nalepka, R. F.; and Thompson, F. J.: Influence of the Atmosphere on Remotely Sensed Data. Proceedings of the Photo-Optical Instrumentation Engineers, 51, 1974, pp. 101-114.

8. Turner, R. E.: Atmospheric Effects in Multispectral Remote Sensor Data. ERIM Report 109600-15-F, May 1975.

9. Fraser, R. S.; Bahethi, O. P.; and Al-Abbas, A. H.: The Effect of the Atmosphere on the Classification of Satellite Observations to Identify Surface Features. Remote Sensing of Environment, 6, 1977, pp. 229-249.

10. Valley, S. L. ed: Handbook of Geophysics and Space Environments. McGraw-Hill Book Co., Inc., 1965.

11. West, G. S., Jr.; Wright, J. J.; and Euler, H. C.: Space and Planetary Environment Criteria Guidelines for Use in Space Vehicle Development, 1977 Revision. NASA TM-78119.

12. Gates, D. M. ...pectral Distribution of Solar Radiance at the Earth's Surface. Science, 4 February 1966, Vol. 151, No. 3710, pg. 523.

13. Selby, J. E. A.; and McClatchey, R. A.: Atmospheric Transmittance from 0.25 to 28.5 μm: Computer Code LOWTRAN3. AFCRL-TR-75-0255, 5 May 1975.

14. Lowe, D. S.: Spectral Signatures and Measurements. University of Michigan, presented as part of UCLA Remote Sensing Course, 5 to 16 August 1968.

15. McClellan, W. D.; and Meiners, J. P.: Spectral Reflectance Studies on Plants. Proceedings of Second Symposium on Remote Sensing of Environment, October 1962.

16. Olson, C. E., Jr.; and Good, R. E.: Seasonal Changes in Light Reflectance with Forest Vegetation. Photogrammetric Engineering, Vol. 28, No. 1, 1962, pp. 107-114.

17. Polcyn, F. C.: Investigations of Spectrum Matching. Sensing in Agriculture, Volume 1, Final Report, May 1964 through March 1967, University of Michigan, November 1967.

18. Gates, D. M.: Characteristics of Soil and Vegetated Surfaces to Reflected and Emitted Radiation. Bureau of Standards, Proceedings from Third Symposium on Remote Sensing of Environment, November 1965, pp. 513-600.

19. Norwood, V.; and Lansing, J. C., Jr.: Multispectral Point Scanner Study and Multispectral Scanning Point Scanner Camera System. Hughes Ref. No. B6872, SSD 00038R, 30 January 1970.

20. Johnson, P. L.; ed.: Remote Sensing in Ecology. University of Georgia Press, 1969.

21. Malila, W. A.; Cicone, R. C.; and Gleason, J. M.: Wheat Signature Modeling and Analysis for Improved Training Statistics. NASA CR-ERIM 109600-66-F, May 1976.

22. Christenson, D.; Gordon, M.; Kistler, R.; Kriegler, F.; Lampert, S.; Marshall, R.; and McLaughlin, R.: MIDAS, Prototype Multivariate Interactive Digital Analysis System for Large Earth Resources Surveys; Volume I: System Description. NASA CR-2730, April 1977.

23. Wheeler, S. G.; and Ingram, D. S.: Approximation for the Probability of Misclassification. Pattern Recognition, 1976, Volume 8, pg. 119.

24. Wacker, A. C.; and Landgrebe, D. A.: Boundaries in Multispectral Imagery by Clustering. 1970 IEEE Symposium on Adaptive Processes (9th), Decision and Control, December 7-9, 1970.

25. Detchmendy, D. M.; and Pace, W. H.: A Model for Spectral Signature Variability for Mixtures. In Remote Sensing of Earth Resources, Vol. 1, ed. by F. Shahrokhi, March 13-14, 1972, pg. 596.

26. Su, M. Y.: The Composite Sequential Clustering Technique for Analysis of Multispectral Scanner Data. NASA CR-128999, October 1972.

27. Jayroe, R. R., Jr.: Unsupervised Spatial Clustering with Spectral Discrimination. NASA TN D-7312, May 1973.

28. Kan, E. P.; Holley, W. A.; and Parker, H. D., Jr.: The JSC Clustering Program ISOLS and Its Applications. Machine Processing of Remotely Sensed Data. October 16-18, 1973.

TABLE I.- COMPUTATIONAL REQUIREMENTS FOR THE CLASSIFICATION OF EACH SIGNAL PATTERN

Decision Topology	Decision Process	Number of Multiplications and of Additions[1]
Single-level	MSD[2]	$2LJ \leq 2MNJ$
	MLR[3]	$\frac{L}{2}(J^2 + 3J) \leq \frac{MN}{2}(J^2 + 3J)$
Two-level with supervisory classifier	MSD for both levels	$2MJ_1 + 2NJ_2$
	MLR for both levels	$\frac{M}{2}(J_1^2 + 3J_1) + \frac{N}{2}(J_2^2 + 3J_2)$
	MSD for first level, and MLR for second level	$2MJ_1 + \frac{N}{2}(J_2^2 + 3J_2)$

[1] The number of multiplications and additions are equal to each other for both decision processes. (From ref. 23 for single-level topology.)

[2] Mean-square distance.

[3] Maximum-likelihood ratio.

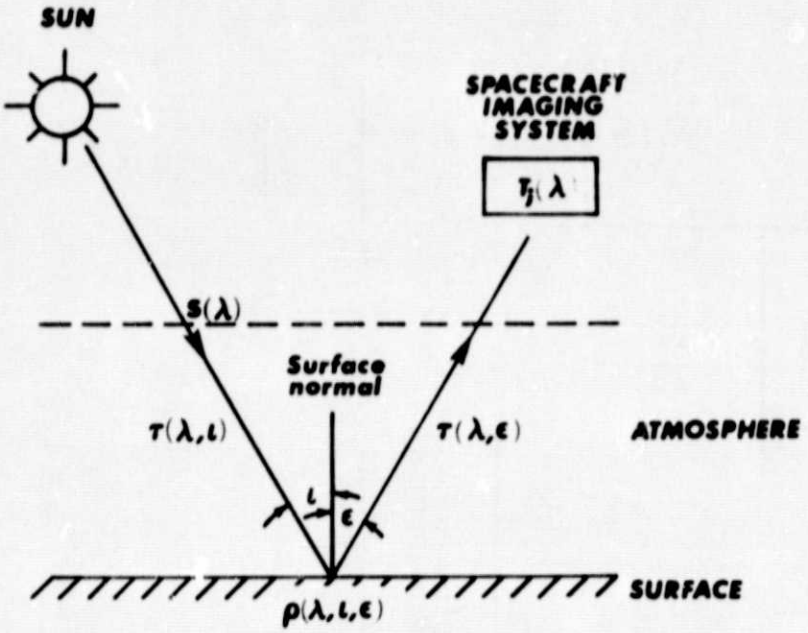

Figure 1.- Lighting and viewing geometry.

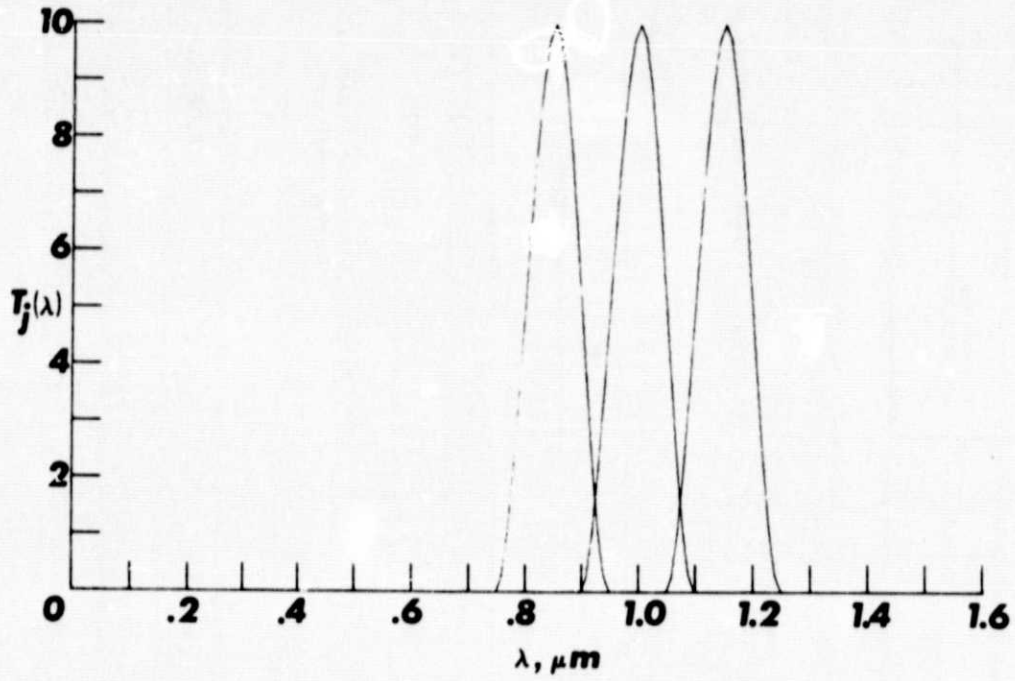

Figure 2.- Spectral response.

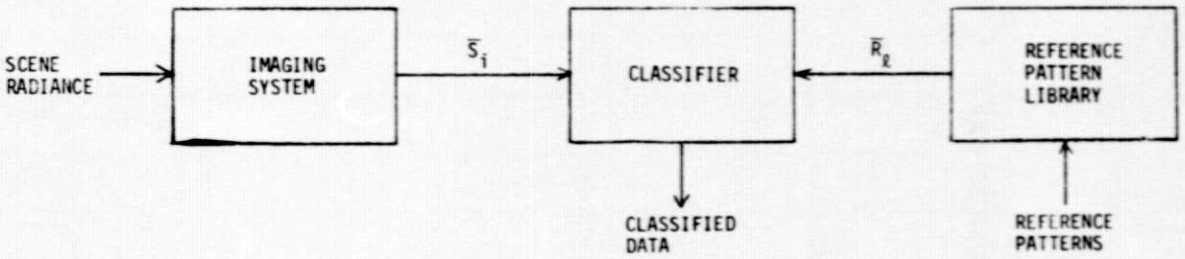

(a) Model 1: Common classification process.

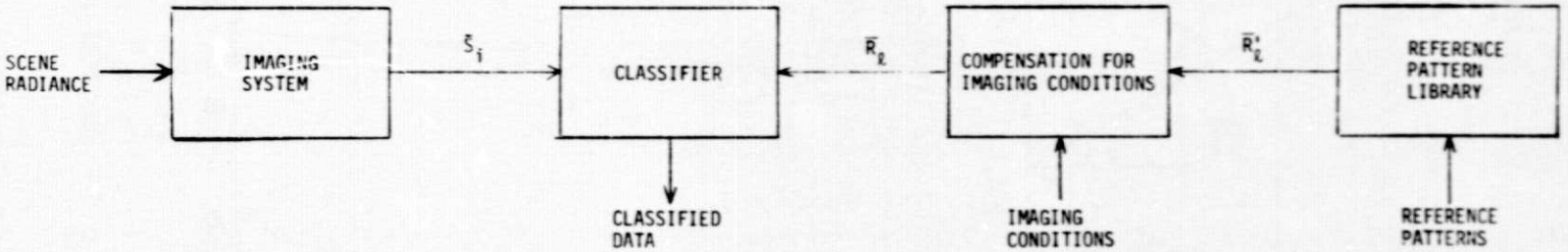

(b) Model 2: Classification process with compensation for imaging conditions.

Figure 3.- Statistical models.

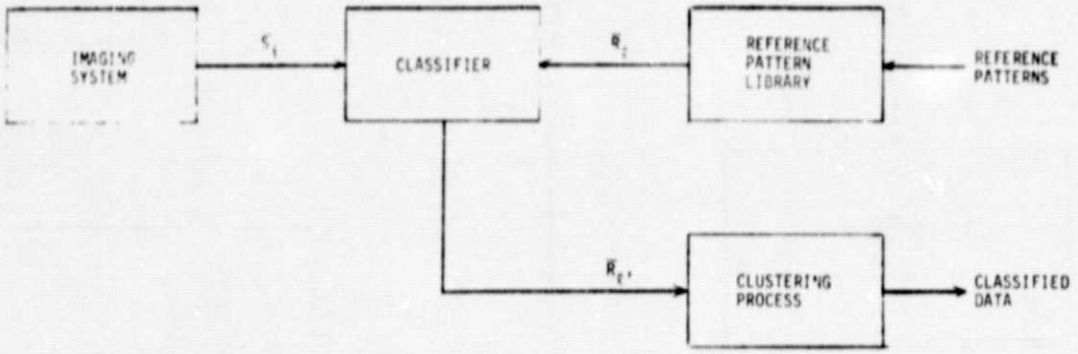

(a) Single-level decision process.

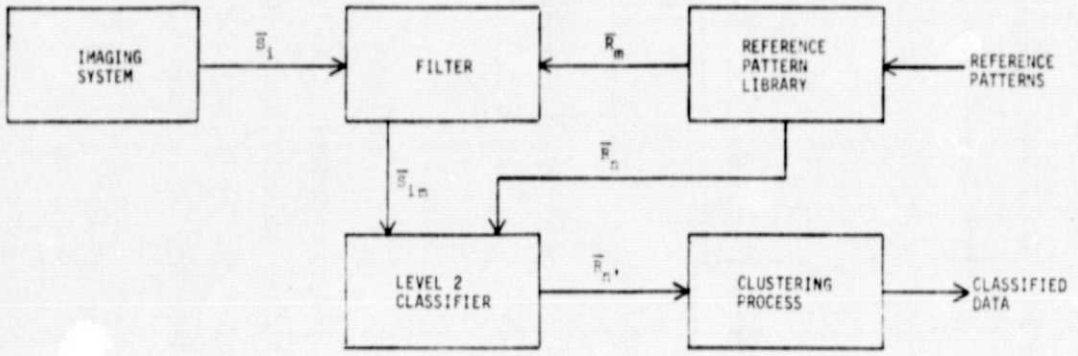

(b) Two-level decision process with filter.

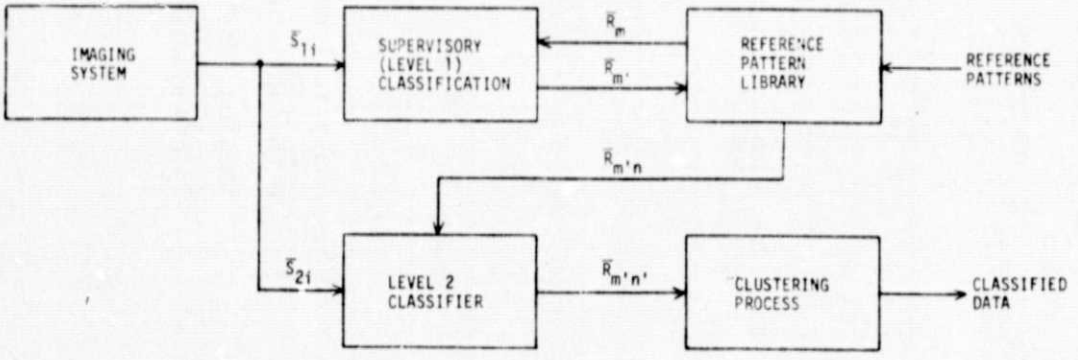

(c) Two-level decision process with supervisory classifier.

Figure 4.- Classification topologies.

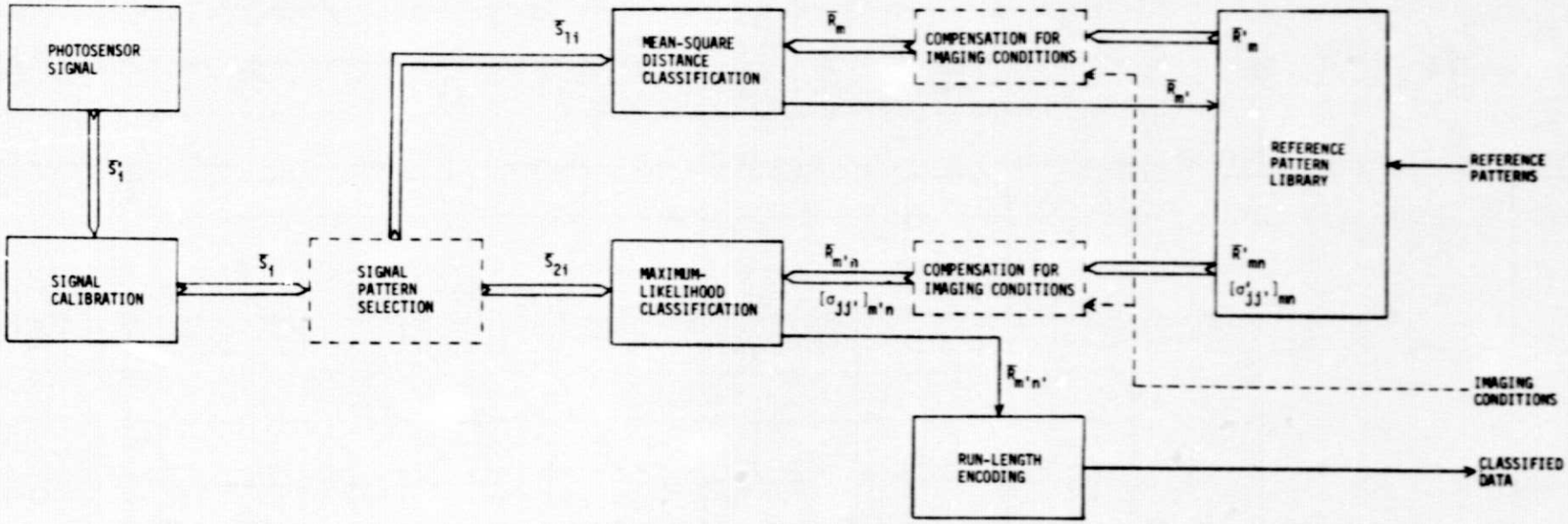

Figure 5.- Analytical model. The topology represents two-level classification with (optional) spectral channel selection and compensation for imaging conditions. The model can also simulate single-level classification with mean-square distance or maximum-likelihood decision.

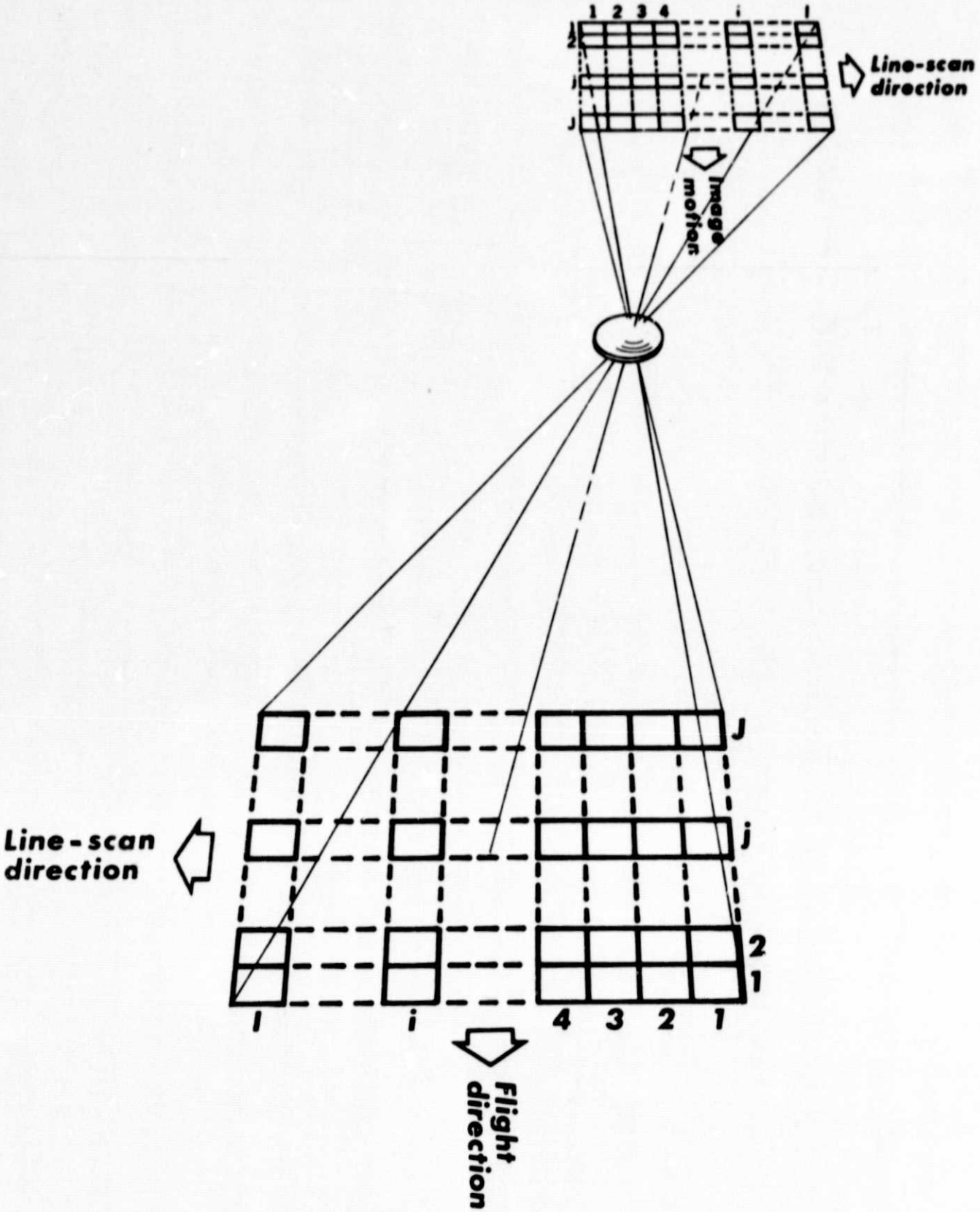

Figure 6.- Imaging geometry.

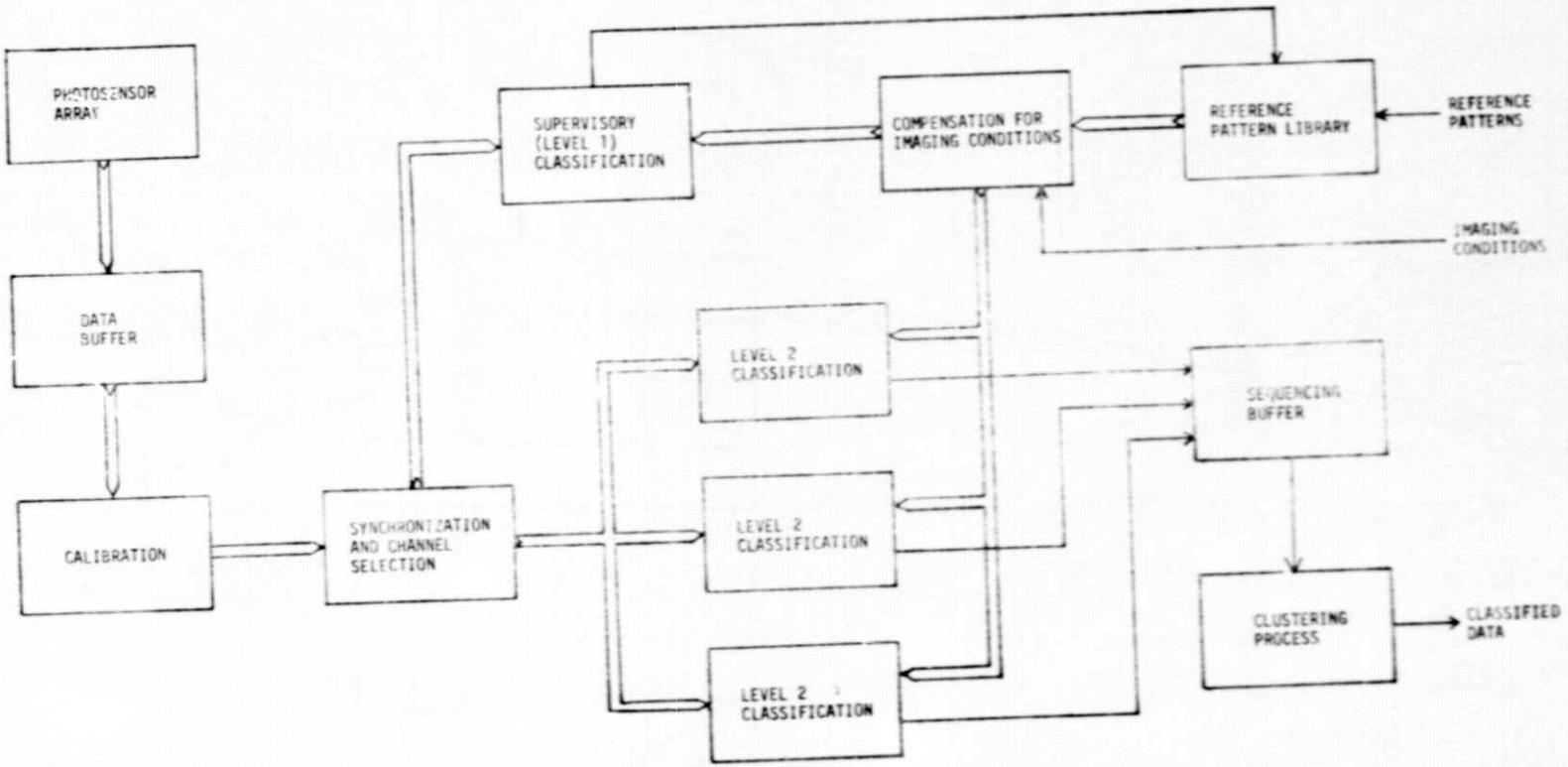

Figure 7.- Example spacecraft system topology.

1. Report No.	2. Government Accession No.	3. Recipient's Catalog No.
NASA TM-78795		

4. Title and Subtitle	5. Report Date
ANALYTICAL MODELS AND SYSTEM TOPOLOGIES FOR REMOTE MULTISPECTRAL DATA ACQUISITION AND CLASSIFICATION	August 1978
	6. Performing Organization Code

7. Author(s)	8. Performing Organization Report No.
Friedrich O. Huck, Stephen K. Park, Ernest E. Burcher, and W. Lane Kelly, IV	
	10. Work Unit No. 506-18-21-02
9. Performing Organization Name and Address	11. Contract or Grant No.
NASA Langley Research Center Hampton, VA 23665	
	13. Type of Report and Period Covered
12. Sponsoring Agency Name and Address	Technical Memorandum
National Aeronautics and Space Administration Washington, DC 20546	14. Sponsoring Agency Code

15. Supplementary Notes

16. Abstract

This paper presents simple analytical models of the radiometric and statistical processes that are involved in multispectral data acquisition and classification, and basic system topologies which combine remote sensing with data classification. These models and topologies offer a preliminary but systematic step towards the use of computer simulations to analyze remote multispectral data acquisition and classification systems.

17. Key Words (Suggested by Author(s))	18. Distribution Statement
Multispectral data acquisition Multispectral data classification Remote sensing	Unclassified - Unlimited Subject Category 35

19. Security Classif. (of this report)	20. Security Classif. (of this page)	21. No. of Pages	22. Price*
Unclassified	Unclassified	37	$4.50

* For sale by the National Technical Information Service, Springfield, Virginia 22161